Comparing physical and chemical properties of soot from laboratory tests and heavy-duty engines used in field operations.

A. Pacino[1], A. La Rocca[1], J. Smith[2], J. Berryman[2], M. Fowell[2], A. Cairns[1], M.W. Fay[3]

[1]Powertrain Research Centre, The University of Nottingham,
[2] Infineum UK Ltd
[3] Nanoscale and Microscale Research Centre, University of Nottingham, UK

Abstract

Morphology, nanostructure, and composition of soot extracted from the oil sump of different heavy-duty engines operated under dynamometer and field conditions were investigated. Soot characteristics were then compared to a carbon black sample. Soot was extracted from used oil for Transmission Electron Microscopy (TEM) analysis. Energy Dispersive X-Ray (EDX) and X-ray photoelectron spectroscopy (XPS) analyses were also performed to assess soot composition. Two soot classes, I and II, can be identified based on their appearance under the TEM. Carbon black and class I particles have graphitic structures, while class II samples have a more sludge-like appearance. Similar aggregate sizes were observed among the samples. In all samples, the primary particle size distribution ranges from 16 nm to 22 nm in terms of mean diameter. Differences in the length and tortuosity of the graphitic fringes between the samples were observed. The findings suggest a greater degree of interaction between class II samples and the lubricating oil, and consequently, a different wear behaviour may be expected depending on the specific soot characteristics.

Keywords

Diesel engine, soot-in-oil, transmission electron microscopy (TEM), nanostructure, morphology

1. Introduction

The diesel engine currently remains the most widely used solution for powering heavy-duty applications and off-road machinery [1]. Diesel trucks accounted for 97.9% of the market in 2019 [2]. The diesel engine is also the primary source for transportation in the marine sector [3]. The demand for better fuel economy and legislation-driven requirements have led to the introduction of advanced engine technologies in the last few decades [4, 5] (e.g. advanced combustion control strategies [4],

turbocharging [6], after-treatment devices [7], and exhaust gas recirculation (EGR) [8-10]), leading, in some cases, to increased soot production and oil contamination. These soot nanoparticles in oil shorten engine life due to increased wear of components and increase fuel consumption due to higher friction [11, 12].

Despite various attempts to fully understand the fundamentals of soot-induced wear in ICEs, the actual mechanism remains unknown [13]. The relationship between engineering practice and the application of analytical techniques such as TEM, XPS, and Raman is rooted in the latter's capacity to improve knowledge of soot characteristics, behaviour, and interactions with wear and lubricating oil [13, 14]. These tools play a crucial role in enhancing the understanding of soot and in developing effective strategies for mitigating their adverse effects [15].

This paper aims to explore the possibility that various kinds of soot, characterized by unique properties, have been employed in diverse experimental studies, leading to varied and conflicting results.

Soot nanoparticles form in high temperature fuel-rich regions due to pyrolysis, with small hydrocarbon branches forming acetylene precursors and then polycyclic aromatic hydrocarbons (PAHs). These PAHs stick together, seeding the formation of soot. Coagulation and surface growth leads to the formation of a primary particle characterised by an inner core surrounded by graphite carbon sheets, generally known as the outer shell. These primary particles stick to one another forming branched aggregates [16]. While most of the produced particulate matter leaves the combustion chamber with the exhaust gas, a small percentage of soot is transferred to the engine oil via the blow-by gases and thermophoretic mechanisms [11]. The latter is defined as particle motion caused by a temperature gradient due to molecules with higher energy levels pushing particles to the cold side [17, 18]. Despite oxidation occurring throughout the entire process, soot-in-oil experiences less oxidation than the exhaust counterpart due to its early migration into the lubricating oil [19].

The degree of atomic organization within a carbon material is referred to as nanostructure [20]. Carbon atoms typically bond together to form nanometric formations (called fringes) in which they can locate either within the basal plane or the edge sites [21]. The carbon edge sites are commonly considered to be 100-1000 times more reactive than those in the basal plane [21, 22]. This is due to their high exposure to oxygen attack and the abundance of unpaired sp^2 electrons, which allow these atoms to easily bond with oxygen [20, 23, 24]. Long carbon fringes lead to fewer edge atoms, resulting in less reactive soot. Aside from fringe length, fringes' tortuosity is commonly used to characterise the nanoscale ordering in a carbon material. This is defined as the ratio of the geodetic to Euclidean distance between the outer edges of the carbon fringe [25]. More tortuous graphene

layers lead to more defective / reactive nanostructure due to oxygen-induced graphene sheet distortion [23, 24, 26, 27]. Thus, sizes, orientation, and arrangement of the carbon lamella characterise the carbon structure. The chaotic configuration of lamellae is usually referred as "turbostratic" [28]. As a result, fringes' length and tortuosity are good indicators by which the structure type and its disorder can be quantified [29, 30].

It has been reported that soot particulates have an impact on engine wear [11, 13, 31-36], friction coefficient [12, 37-39] and oil viscosity [12, 37, 39-41]. Different mechanisms have been established for soot/lubricant interactions and many theories have been suggested over the last 40 years [13]. The literature reveals a well-established but complex, and not comprehensively understood, relationship between soot nanoparticles and engine lubricant oils. Gautam [32] found a proportional relationship between soot-in-oil contamination and wear of engine components. How exactly these are related, and consequently, how this problem can be avoided, has not been precisely defined. The complexity of the relationship between soot particles and lubricant oil behaviour is exacerbated by several supplementary variables that differ among the investigations (engine, fuel, operating conditions, oil properties, oil formulation, type of contaminant, soot surrogates). A soot surrogate was used by Green to investigate the impact of nanoparticles on engine wear [37]; this carbon black enhances wear, and the mechanism shifts from abrasion to starvation with increasing concentration. According to Clague [42], carbon black can be used to mimic wear from soot. Conversely, Antusch [38] suggests that dyno-derived engine soot is more prone to cause wear than carbon black.

Commercially available carbon black (CB) has often been used as a soot surrogate [38, 40, 42-44], with a view of achieving repeatable results, given that soot might vary in graphitization and particle dimensions due to engine operating conditions [45, 46]. Clague [42] observed primary particles size in the range of 30-50 nm and similar structural order between engine soot and carbon black. Substantial differences were found on their elemental composition and surface chemistry. Carbon black particles showed more carbon content, reduced ash, and lower volatile component content. Wedlock [47] pointed out that carbon black aggregates are comparable to those of engine soot, suggesting carbon black is a realistic soot surrogate. Antusch [38] linked the reduced wear rate to the lower reactivity of carbon black compared to dyno-derived soot. Jaramillo [48] compares three different carbon blacks to soot collected from a forklift (field-derived soot); suggesting that carbon black is not always more graphitic than soot. Yehliu [29] pointed out that carbon black nanostructure can be altered by different heat treatments.

The interaction between oil additive and soot is known to depend strongly on both the physical (*e.g.,* size, shape, surface area etc.) and chemical (*e.g.,* surface chemistry, nanostructure etc.) properties of soot nanoparticles. Rounds [35] suggested preferential absorption of the anti-wear additive on dyno-derived soot rather than on the metallic surfaces. On the contrary, Hosonuma [33] and Kawamura [34], found no evidence of anti-wear additive performance being depleted by dyno-derived soot and field-derived soot respectively. By means of tribological and field tests, Corso [31] confirmed a competitive chemical adsorption of anti-wear additives on the contact surfaces of valve train materials in field and tribological tests. Three-body abrasive wear, according to Li [49], takes place for lubricant films thinner than the soot aggregate size from a Cummins M11 test. The reported wear scar widths matched the size of primary particles, supporting this hypothesis. Other studies have revealed that the hardness of soot ranges between 0.3 and 8 GPa [50, 51], resulting in the range of forged steel and cast iron and thus suggesting its potential abrasive action on engine components [50, 51].

It has also been suggested that soot particles cause oil starvation, and consequently wear due to metal-metal contact. Green [44] observed a transition from abrasive wear to starvation, due to carbon black contamination clogging the entrance of the contact zones. Similarly, Yoshida observed lubricant starvation and high wear rates when soot aggregates are greater than the oil film thickness [52]. Recently, Salehi [40] and Olomolehin [53] proposed a corrosive-abrasive mechanism in which wear is caused by the chemical reaction of the zinc dialkyl dithiophosphates (ZDDP) anti-wear agent with the metallic surface, followed by rapid abrasive removal of the generated phosphorus-based tribofilms by carbon black particles. Similarly, Booth [43] observed increased wear rates in pin-on-disc tribometer experiments when both ZDDP and carbon black were present in the oil, suggesting the latter was responsible for the abrasion mechanism of the anti-wear film.

The research conducted so far suggests that the amount of soot in the oil impacts engine wear, although the wear rates may vary depending on soot characteristics. Soot properties such as particle morphology, nanostructure, and chemistry are therefore crucial in defining the soot-induced wear process. For instance, Berbezier [54] reported increased wear rates and decreased anti-wear capabilities of the oil with increasing carbon black primary particle size. Similarly, Mainwaring [55] observed more severe wear behaviour for soot with larger primary particles. Antusch [38] established that the wear rate also depends upon soot surface chemistry and reactivity. The authors proposed various nanostructures to alter the reactivity of engine soot. Similarly, Uy [56] discovered that amorphous carbon leads to increased wear during four-ball wear tests. The interaction between oil additives and engine soot is dependent on its chemical reactivity, and thus on its nanostructure [15]. Thus, the oils performance and wear mechanism are intimately related to the physicochemical

properties of the particulate matter. To design high-quality engines and oil additives, research into soot properties is required, which necessitates the use of advanced analysis techniques.

Soot-in-oil characterization has been the subject of many investigations [15, 21, 28, 30, 38, 56-64]. For example: soot nanoparticles have been commonly investigated by means of Transmission Electron Microscopy (TEM) [15, 21, 38, 57, 65]. Antusch [38] compared images of carbon black and dyno-derived soot, concluding that carbon black primary particles are larger. Esangbedo [15] analysed dyno-derived soot noticing a more branched aggregate morphology for soot derived from an engine running with EGR. La Rocca [57] studied the impact of sample preparation on generating artefacts in aggregate size distribution. Vander Wal [21] used TEM to produce high-resolution images and studied flame soot reactivity as a function of fuel type. Haffner-Staton [65] employed TEM to compare the 2D and 3D morphology of soot in-oil particles extracted from a light-duty gasoline engine operated under field conditions. They found particles size differences of 20% to 35% between the two techniques.

Energy-dispersive X-ray spectroscopy (EDX) has been used to investigate the chemical composition of soot [28, 61, 62, 64]. Patel [61] was able to prove the presence of crystalline patterns embedded in the soot nanostructure. Similarly, EDX measurements conducted by Pfau [62] showed crystalline structures and presence of oil additives on field-derived soot particles. Sharma [28] employed EDX coupled with TEM to investigate the differences between engine and exhaust soot. They concluded that the crankcase soot contains more oil additives than the exhaust counterpart. EDX investigations have also been conducted by Vyavhare [64] to assess the impact of oil additive package on soot chemistry in standard test-derived oil drains.

X-ray photoelectron spectroscopy (XPS) has proven to be a reliable method to get information about the surface chemical composition [30, 38], and reactivity [56, 60] of carbonaceous materials. Unlike EDX, which provides information about elemental composition of a broad volume of the sample, XPS is a surface-sensitive technique that utilizes the low-energy X-ray beam to probe the surface elemental composition of a carbon material [66]. Using the technique Antusch [38] found considerable differences in soot surface composition among carbon black, diesel, and gasoline soot, with the latter showing the highest amount of oxygen functional groups and reactivity among the samples. Uy [56] also characterized dyno- and field-derived soot particulates by means of XPS spectroscopy. They found a more oxidised exhaust soot in comparison to the oil drain samples. Traces of oil additive components were found by Kim and co-workers on sooted oil samples extracted from a light-duty diesel engine operated under dyno test conditions [59]. Muller employed XPS to establish a correlation between the nanostructure, the bonding state of the carbon atoms, and the oxygen content for carbon black and dyno-derived diesel soot samples [60]. Similarly, Vander Wal linked the nanostructure with the carbon

bonding sp^2/sp^3 state of soot extracted from different sources (diesel engine, oil-fired boilers, jet engine) [30].

In addition to the previous techniques, Raman spectroscopy is often used for characterizing soot nanostructure [15, 56, 58, 62, 63]. Raman is sensitive to molecular structure and can therefore be used to quantify the degree of graphitization in carbon-containing materials. By means of Raman Spectroscopy, Uy has discovered amorphous regions in the nanostructure of crankcase and exhaust soot from dyno and field engine tests [56]. Esangbedo [15] used Raman spectroscopy to determine that a more graphitic soot leads to a quicker loss of viscosity control during dynamometer engine tests. The greater the graphitic soot, the lower the oxygen functionalization, resulting in viscosity control loss due to less interaction with oil dispersants. Similarly, Al-Qurashi reported a reduced efficacy of engine dispersant and a consequent viscosity increase in presence of "un-reactive soot" [26]. Comprehensive experimental research on several carbon materials, including highly oriented pyrolytic graphite and amorphous carbon formations, was conducted by Escribano [58]. The study reported a general agreement between the carbon nanostructure and the Raman results. Pfau observed a linear correlation between Raman defects/graphitic ratios and fringes parameters (namely length and tortuosity) for both engine soot and carbon black material [62]. Sadezky [63] used Raman spectroscopy coupled with X-ray diffraction measurements to assess the statistical uncertainties of Raman curve fitting for a carbon material. Different types of soot can be therefore distinguished based on the degree of graphitization in the material, however, achieving accurate and meaningful comparisons between samples necessitates a meticulous setup and precise calibration [67].

A variety of techniques have been previously employed to separate soot particles from the engine oil. Pfau [62] diluted oil samples in heptane and transferred small amounts onto TEM carbon grids after centrifuging and ultrasonic bathing. Similarly, Uy [56] diluted sooted oil drains in hexane. Then, four runs of centrifugation were performed to remove any oil contamination. Likewise, Fay [68] diluted oil samples in heptane and transferred small amounts onto TEM grid after five stages of centrifugation at 14,000 rpm for 90 minutes. However, it has also been shown that the centrifugation process can alter the size and shape of soot agglomerates [57].

Many morphological parameters have been employed in literature to classify particles according to their size. La Rocca found clusters and chain-like structures with an average hydraulic diameter of 100 nm in diesel soot-in-oil samples [69]. Similar agglomerates were found by Clague [42] in their investigation on engine soot and carbon black. In a later investigation, La Rocca [70] measured oil soot from a GDI engine, showing a mixture of clusters and chain-like structures with a mean skeleton length of 153 nm. Similarly, diesel soot showed an average skeleton length of 131.8 nm, composed

of spherical primary particles of 12–40 nm [57]. In their work, Neer and Koylu [71] identified soot particles with a gyration diameter up to 0.2 μm.

The knowledge gained so far suggests a discrepancy in wear results found in the research. Moreover, soot-in-oil literature to date is often limited to a rather small number of samples and analysis published in individual papers. Primary focus is given to particle morphology with limited emphasis to the chemical information. The reactivity of soot is often measured using chemical techniques, but multiple setups, operators and conditions might affect sample comparability. Similarly, quantifying nanostructure using fringe analysis and comparing results from multiple authors can be challenging. This study aims to address these gaps by undertaking a comprehensive characterization of soot originating from different heavy-duty dyno, field engines and a carbon black. Through a systematic approach, statistical analyses are performed, enabling meaningful comparisons among samples. TEM was employed for the quantitative assessment of the soot morphology and nanostructure. EDX and XPS were used to determine the chemical composition of soot. This work interconnects the morphology, nanostructure, and chemistry of soot-in-oil particles—aspects that are frequently overlooked when examining wear mechanisms. These features are linked to the possible wear mechanisms with a view of explaining the discrepancy in soot-induced wear observations found in the literature.

2. Experimental

2.1 Samples Description

Three field-derived soot samples, five laboratory dyno-derived soot samples and one flame-generated carbon black sample were analysed in this study. The details of those samples are given in Table 1.

Sample A was drained from the oil sump of a Euro 6 compliant 8 L engine operated for 109,061 km.

Sample B and C were collected from engine oil drains of two heavy-duty trucks equipped with a 13 L engine, with turbocharger and exhaust gas recirculation (EGR) systems, meeting the Euro 6D emission specification. Oil samples were taken at 60,000 km and 140,000 km, respectively.

Oil drain samples D and E were obtained from two diesel engines with the same displacement (13 L), turbocharging, and bowl design. These engines meet Euro 6D and 6E emissions standards, respectively. The engines were tested on a dyno test bed, which replicated heavy-duty field applications.

Sample F was obtained from a dyno engine test. The test uses a heavy-duty diesel engine with 5.9 L displacement, equipped with exhaust gas recirculation (EGR) system operating to a 350-hour test procedure. The test method consists of 17 min warm-up, an 80 h break-in, and a 350 h test cycle.

First, the engine is operated with retarded fuel-injection timing to generate excess soot, then the engine is run at cyclic conditions to induce valve-train wear.

Sample G comes from a 11 L heavy-duty engine equipped with EGR system. The test duration consists of 200 hours. High-soot loading production and stop-and-go operations simulate real-world field service during the test.

Sample H was obtained from a heavy-duty dyno test. An 11 L diesel engine is equipped with EGR, and variable geometry turbocharger. The test procedure involves 30 minutes of oil flushing, followed by 252-hour test at constant speed and load conditions.

At the conclusion of every test or drain interval, approximately 75 mL of oil sample was carefully drawn from the sump of the respective engine for soot analysis.

Sample L is a commercially available carbon black 'Cabot Mogul L', previously employed as a surrogate in other investigations in the literature [56, 72].

For all test cell-based samples, the engine was running the durability drive cycle, i.e typically full load sweeps in the 900 – 2000 rpm range, followed by a standing for 7 minutes. Oil temperature was kept at 125 ºC during the running cycle. For field samples, oils were taken at engine-off conditions. All tests oil samples are taken using a sampling system (i.e. a tube plumbed into the oil sump), extracted from the deep part of the sump.

2.2 Samples Preparation

After gently mixing the oil samples for a minute, 0.5 ml of the oil was extracted using an Eppendorf pipette and diluted with the solvent and analysed. Measuring known size distributions and concentrations of CB dispersed in engine oil has previously demonstrated the robustness of this method [73].

2.2.1 Transmission Electron Microscopy (TEM)

Soot was isolated from engine drain oils using a solvent extraction process. The dilution was carried out with an appropriate amount of heptane depending on the soot content in the sample. Small amounts of soot suspension in heptane were transferred onto carbon coated TEM grids. Following deposition, the heptane evaporates leaving the soot particles on the grid. The grids were washed with diethyl ether to remove any remaining oil contamination from the sample [70]. Further vaporization of the solvent was then promoted by subjecting the sample to close-to-vacuum conditions prior to the TEM analysis. TEM was used for acquisition of high-resolution images of soot on copper mesh grid consisting of graphene oxide support film and holey amorphous carbon layer. A JEOL 2100F TEM microscope with

a Gatan Orius CCD camera, based in the Nanoscale and Microscale Research Center (nmRC) at the University of Nottingham was used to perform the imaging. An incident electron beam voltage of 200 kV was used with various magnifications.

2.2.2 Photoelectron spectroscopy (XPS)

The elemental composition of soot surface was determined by X-ray Photoelectron Spectroscopy (XPS). The soot sample was initially diluted with 75% heptane and distributed between several hermetically sealed 2 mL volume centrifuge tubes. The centrifugation process was performed on the diluted oil/heptane solution at 14,000 rpm for 90 minutes at 25ºC, following the work of Clague [42]. The centrifuged solids were then washed with fresh heptane and sonicated for 10 minutes at 20 °C. The entire process was repeated six times to remove any occluded oil in the sample. The extracted soot in minimal n-heptane solution was deposited on Silicon wafers. Upon evaporation of the heptane in ambient conditions, the wafers were loaded in the high vacuum chamber of the XPS instrument. The base pressure of the spectrometer analyser was 5 x 10^{-9} mbar. The instrumentation used is a Kratos AXIS ULTRA spectrometer, based in the Nanoscale and Microscale Research Center (nmRC) at the University of Nottingham. Photoelectrons were generated using a monochromatic Al kα X-ray source (1486.6 eV), operated at 10 mA emission current and 12 kV anode potential (120 W). Three spectra were acquired using energy steps of 0.5 eV and an acquisition time of 427 ms per step for a total of 20 min per spectra. The area under investigation was 300 x 700 microns giving an average composition across this area. A pass energy of 80 eV was used for the wide spectra acquisition.

Table 1: List of samples analysed in this work.

Sample	TGA Soot wt.%	Test Type	Test Duration	Engine Capacity	Emission Standard	Oil Oxidation A/cm
Sample A	1.02	Field	109,061 km	8 L	EU6 Step C	10.3
Sample B	1.35	Field	62,932 km	13 L	EU6 Step C	16.7
Sample C	1.74	Field	140,803 km	13 L	EU6 Step C	40.2
Sample D	2.3	Dyno	825 h	13 L	EU6 Step D	27.5
Sample E	2.64	Dyno	690 h	13 L	EU6 Step E	97
Sample F	4.9	Dyno	350 h	5.9 L	/	11.1
Sample G	7.00	Dyno	200 h	11 L	/	6.9
Sample H	7.22	Dyno	252 h	11 L	/	10.5
Sample L	/	Carbon Black				

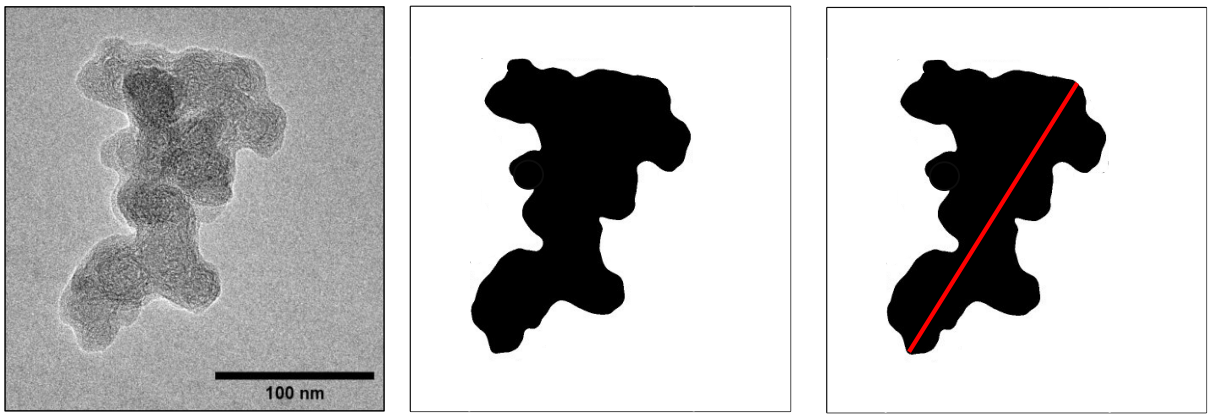

Figure 1: TEM image processing procedure for aggregate size determination: (a) Raw TEM image of a soot aggregate. (b) Binarized image of the example aggregate after applying a user-specified threshold and minor adjustment operations (c) Determination of the maximum Feret diameter

2.2.3 Morphological Analysis

Soot morphology has been investigated using ImageJ, an open architecture image processing software. Several images were analysed for each sample to ensure correct representation of the sample and to account for local variations within. Samples were imaged at several magnifications to observe general soot features, aggregates, and particles' morphology. Morphological information, such as projected area, Feret diameter of the aggregate and size of the primary particles have also been evaluated. A minimum of 100 primary particles was examined per sample, of which the diameter was measured. Primary Particles identification from TEM images was performed by manual detection method. Despite the fact that the manual detection results are affected by operator's experience, a previous study has demonstrated that the fluctuations in the manually derived data can be limited to 3.5% for experienced operators [74]. Aggregates' morphological properties have been evaluated using a semi-automatic image processing method, developed in-house, and coded in ImageJ. Aggregates' identification process includes the manual selection of the soot particles and the automatic threshold adjustment before performing the binarization process. A schematic of the image post-processing procedures is presented in Figure 1.

2.2.4 Structural Analysis

High-Resolution TEM (HRTEM) pictures were used to analyse soot nanostructure within the drain and to determine the degree of order of the graphitic segments that make up the carbonaceous matter [20]. The structural analysis of drain soot samples was performed using a semi-automatic approach based on object tracking and detection in MATLAB and previously applied by Pfau [25]. A minimum of 1000 fringes was obtained per sample. As input to the fringe separation algorithm, the user must specify a region of interest (ROI) in which to evaluate the distance between the lattice fringes. An automatic detection step was instead used to extract fringes' lengths and tortuosity. Statistical distributions are then created from the length and tortuosity data. Additional operational details of the structural analysis are reported in [25].

3. Results

3.1 Morphology

The TEM images of the samples that are being studied are displayed in Figures 2, 3, and 4. The samples are divided into groups according to their provenience, i.e. field or dyno soot. Sample L, a carbon black is conveniently grouped with the dyno soot due to its similarities observed under TEM.

Figure 2 shows the soot morphology found in the samples A, B and C. Soot particulates appear to have a similar morphology and appearance under the TEM. Those samples exhibit aggregates which are less soot-like and more sludge-like in their structures (Figure 2). Most of the particles are amorphous (Figures 2d and f) and experience some degree of decomposition under the electron beam (Figure 2h). Prolonged exposure to the electron beam at normal imaging intensities frequently led to decomposition, suggesting the presence of volatile structures in the material. The mean primary particles diameter was found to be 20 nm, 21 nm, and 22 nm, for samples A, B and C, respectively.

Figure 3 shows the typical particulate morphology found in the samples D and E, consisting of spherical primary particles fused together to form irregular-shaped aggregate structures. Sample D shows soot primary particles connected in bigger soot aggregates. The median primary particles diameter is 16 nm with a standard deviation of 5.4 nm. Most of the particles have a core-shell structure, with a thickness ranging from 4 to 7 nm. Few examples of amorphous carbon can also be observed in the sample (i.e. soot without any long-range order of the carbon lamella [20]). Sample E has an 18 nm

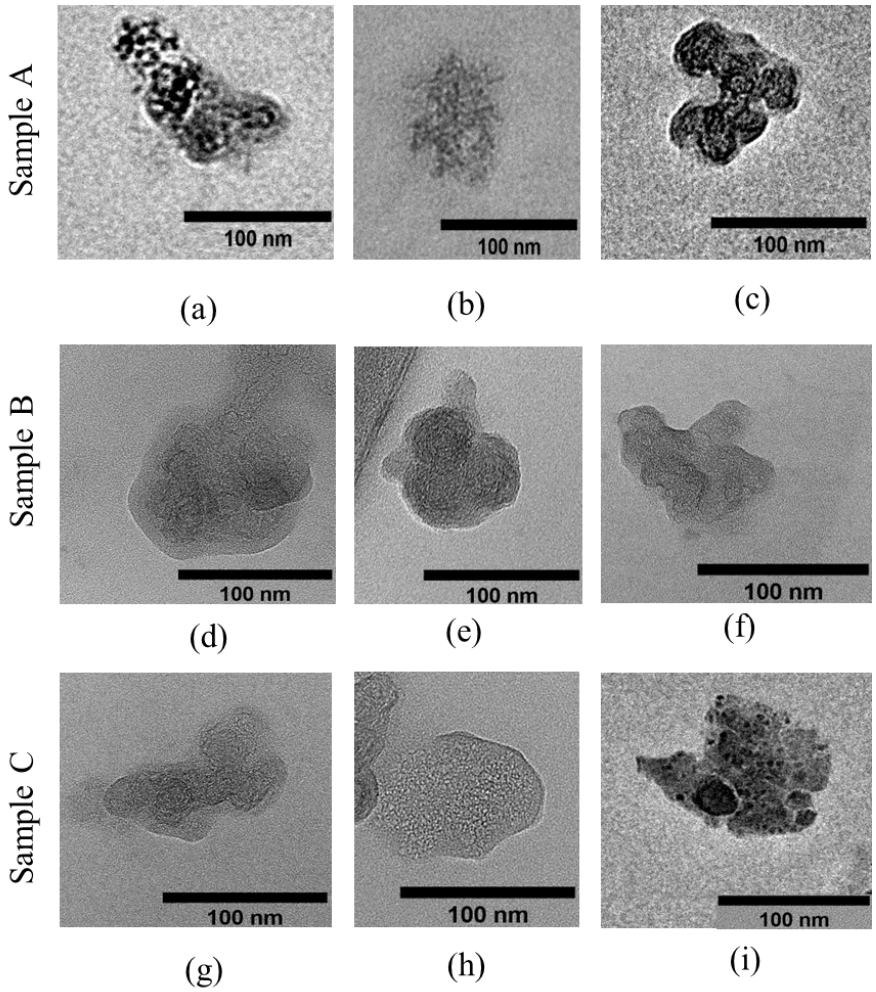

Figure 2: TEM images of samples A,B and C

median primary particles diameter with a 10-28 nm range. Most of the primary particles exhibit an inner core and an outer shell (Figure 3d). The inner core is around 5 nm in diameter with an outer shell 4–12 nm thick. Soot-in-oil aggregates show a modest branched morphology.

Primary particles diameter results are in line with various experimental investigations. La Puerta found an average diameter of 25 nm related to the exhaust soot particles sampled from a diesel engine [75]. La Rocca instead, observed a typical 2 regions structure, i.e. inner core and outer shell, and an average diameter of 20 nm for particles drawn from diesel engine soot-in-oil [57]. Smaller dimensions of the mean particle diameter were found by Su [76]. Their study conducted on diesel exhaust soot showed an average particle diameter in the range 3-15 nm, with a missing outer layer structure. This was ascribed to differences in soot synthesis parameters such as burning temperature, duration, and initial fuel identity. Further investigations on the influence of the operating conditions of the diesel engine

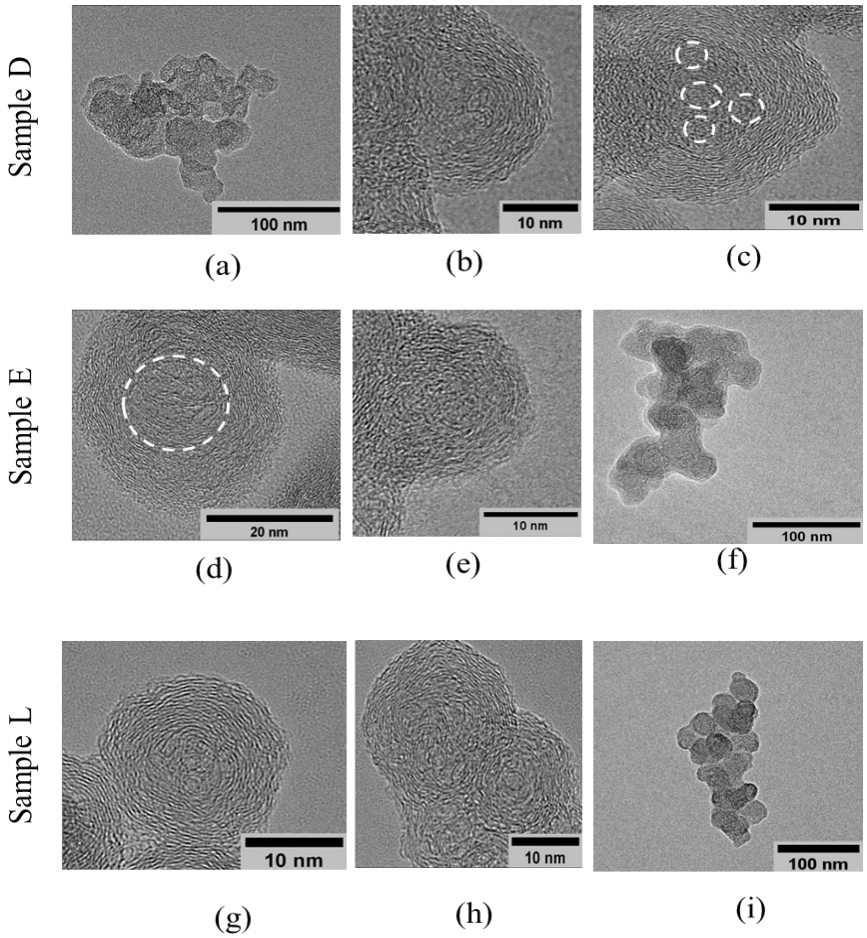

Figure 3: TEM images of samples D, E and L. The circles represent the particle core(s).

on soot have shown that the average diameter of the primary particles is in the range 23.8-34.4 nm [77, 78].

In sample E, the mean Feret diameter (FD) was found to be 141 nm. Aggregates' Feret diameter in sample D spanned from 28 nm to 436 nm. Both samples showed soot aggregates of modest size, with a few examples of amorphous soot and larger particles.

Figure 4 shows some representative TEM images for sample F, G and H. These samples exhibit similar particles size and nanostructure. Sample F has agglomerates up to 2 microns in diameter, with single aggregates ranging from 19 nm to 667 nm. The mean Feret diameter, F, was found to be 252 nm. The carbonaceous particulate matter in the sample looks like a mixture of small aggregates and small agglomerates (Figure 4a and b). Primary particles diameters spanned from 11 nm to 28 nm, with about 90% of the particles less than 21 nm in diameter. Most of the particles are poorly graphitic with multiple-cores structures surrounded by amorphous layers of about 4 nm (Figure 4c). A similar

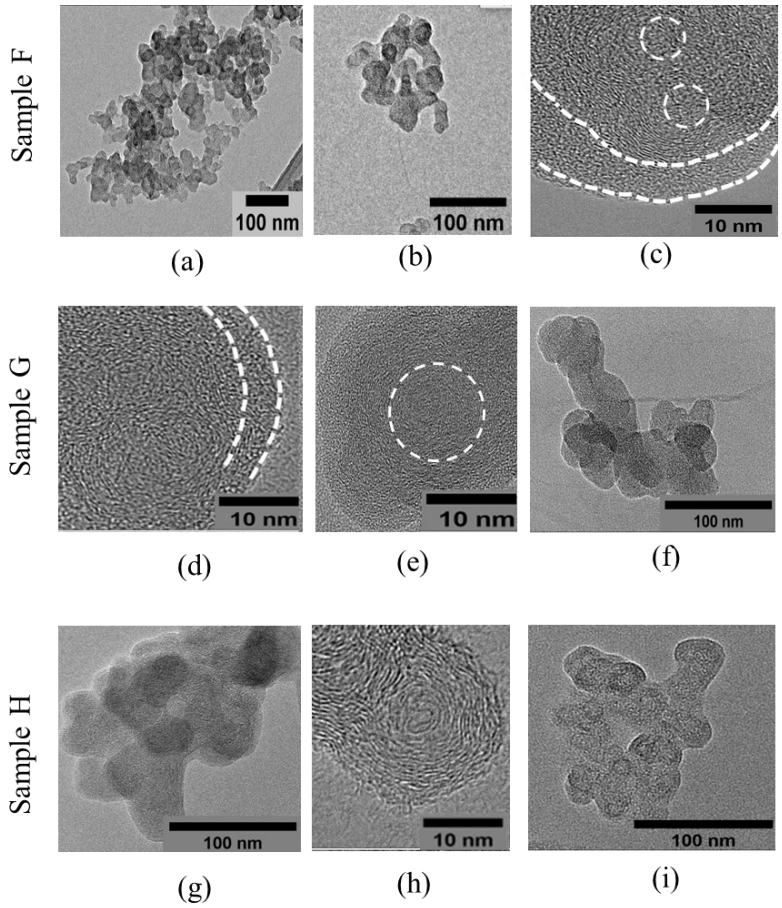

Figure 4: TEM images of samples F, G and H. The dashed lines in the figure indicate the amorphous outer shell, while the circles represent the particle core(s).

amorphous layer was also found in the particles of sample G; however, these mainly exist as single core structures (Figure 4d and e). In this sample, the primary particles' diameter spanned from 11 to 28 nm, with a mean value of 20 nm. Soot aggregates ranged from 75 nm to 650 nm, with 80% of the particles with a Feret diameter in the range 75-275 nm. TEM pictures of sample H show single core-shell primary particles organized in fractal-like soot aggregates of few hundreds of nanometres in size (Figure 4g-i). The centres consist of amorphous nuclei surrounded by graphitic carbon layers. In contrast to samples F and G, no amorphous outer layer is observed here highlighting a more evident long-range graphitic domain in the material. The aggregates' size distribution exhibits an asymmetric shape with particles shifted towards larger sizes from the mode at 175 nm, and the mean Feret diameter is 331 nm.

Sample L exhibited near-spherical primary particles in fractal aggregates of about 100 nm in size. Their structure consists of a central amorphous core surrounded by a largely graphitic outer shell (Figures 3g and h). The mean primary particle diameter was found to be 22 nm. Overall, sample L (CB sample) appearance under TEM looks similar to the dyno-derived soot samples analysed.
Soot aggregates in samples A, B and C (field-derived soot) appears to have a more compact morphology (Figure 2e) as opposed to the modest chain-like geometry of particulates found in the other samples. As such, these particulates are expected to have a greater fractal dimension and a smaller effective volume [15, 79]. Moreover, these samples show significantly darker particulates despite their smaller aggregates' size (Figures 2c and i). This characteristic can be associated either to the presence of a metallic material [70] or to the tridimensionality of soot particles [80].

To understand the chemical composition found in soot particles, an EDX analysis was performed on sample C. Figure 5 shows the EDX spectrum of a black particle found in sample C. Soot particles are mainly composed of carbonaceous material with traces of elements consistent with coming from the oil additive package. Fe originates from engine wear [28, 61]. F, Na, and Si are commonly associated with engine coolant or contamination [62, 81]. Although C and O come mainly from particulate matter, they can originate from the TEM grid and the supporting film, respectively. Due to the use of copper TEM grids, Cu could not be identified using EDX-TEM. The proportion of carbon in soot particles was modest (66 at.%), whereas oxygen was found in abundance. Crystalline material trapped into soot nanostructure was observed by Pfau [62] and their EDX examinations revealed that the embedded particles originated from oil additives and wear compounds. Similarly,

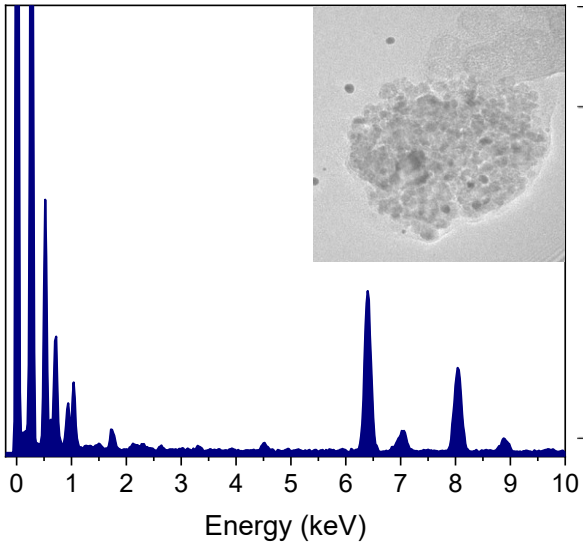

Element At.%	Sample C
C	66.2
O	32.09
Na	0.48
Si	0.13
S	0.03
Cl	0.03
K	0.03
Ti	0.05
Fe	1.13

Figure 5: EDX spectroscopy results of a soot particle in sample C

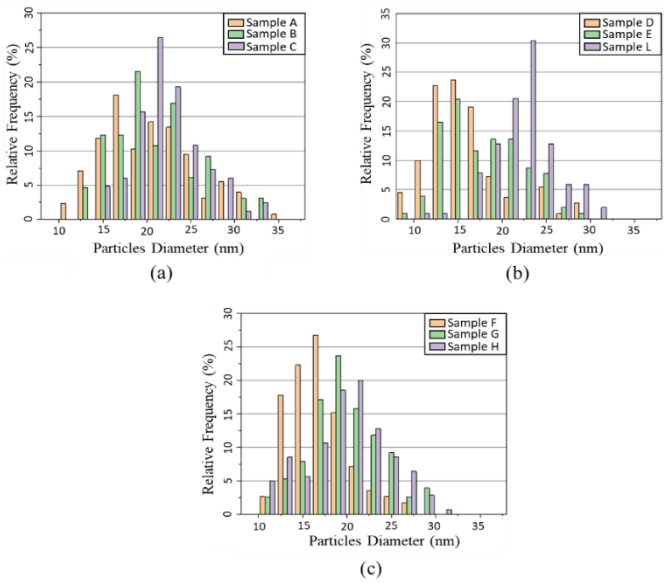

Figure 6: Primary particle diameter distributions for the tested

La Rocca has previously identified dark particles and heavier material on the surface of gasoline engine soot [70]. All the elements detected can been attributed to engine oil additives, coolant, or contamination [56, 62, 81].

The primary particle distributions for all samples are reported in Figure 6. Table 2 summarizes the main TEM results of this study, while Figure 7 shows the main morphological parameters obtained from image analysis. In all samples investigated the aggregates with small surface area and small Feret diameter are the most frequent. Samples F, G and H show the biggest dispersions, probably affected by the small agglomerates within the samples. This is the case of sample F in which those aggregates reach percentages of up to 30%.

A similar consideration can be drawn from the Feret diameter data. Particles with Feret diameter between 75 nm and 125 nm account for more than 50% of the particles in all samples except for sample F in which small degree of agglomeration was found.

Circularity was used to describe the complexity of particles' shape and to differentiate branched from clustered particulates. Statistical results showed that there are considerable differences between the particles' circularity in samples A, B (mean circularity> 0.6) and the other samples. Particles with a circularity greater than 0.6 accounted for about 60% of the aggregates in these samples. The other soot samples show instead similar trend and median values. A similar trend towards chain-like structures is also evidenced by the low particles' circularity found in sample L. Indeed, in this sample, particles with a circularity bigger than 0.6 account for 8% of the

total. As previously stated by Sielicki [82], circularity has proved to be a more effective parameter to evaluate the particles' shape.

Table 2: Summary of TEM observations.

Sample	Mean Feret Diameter nm	Mean Circularity	Mean Perimeter nm	Soot appearance (TEM)	Soot Class
Sample A	122	0.68	351	Sludge-like	II
Sample B	170	0.65	493	Sludge-like	II
Sample C	188	0.56	547	Sludge-like	II
Sample D	158	0.41	579	Graphitic	I
Sample E	141	0.53	425	Graphitic	I
Sample F	252	0.41	923	Graphitic	I
Sample G	231	0.50	759	Graphitic	I
Sample H	331	0.42	1160	Graphitic	I
Sample L	160	0.41	586	Graphitic	I

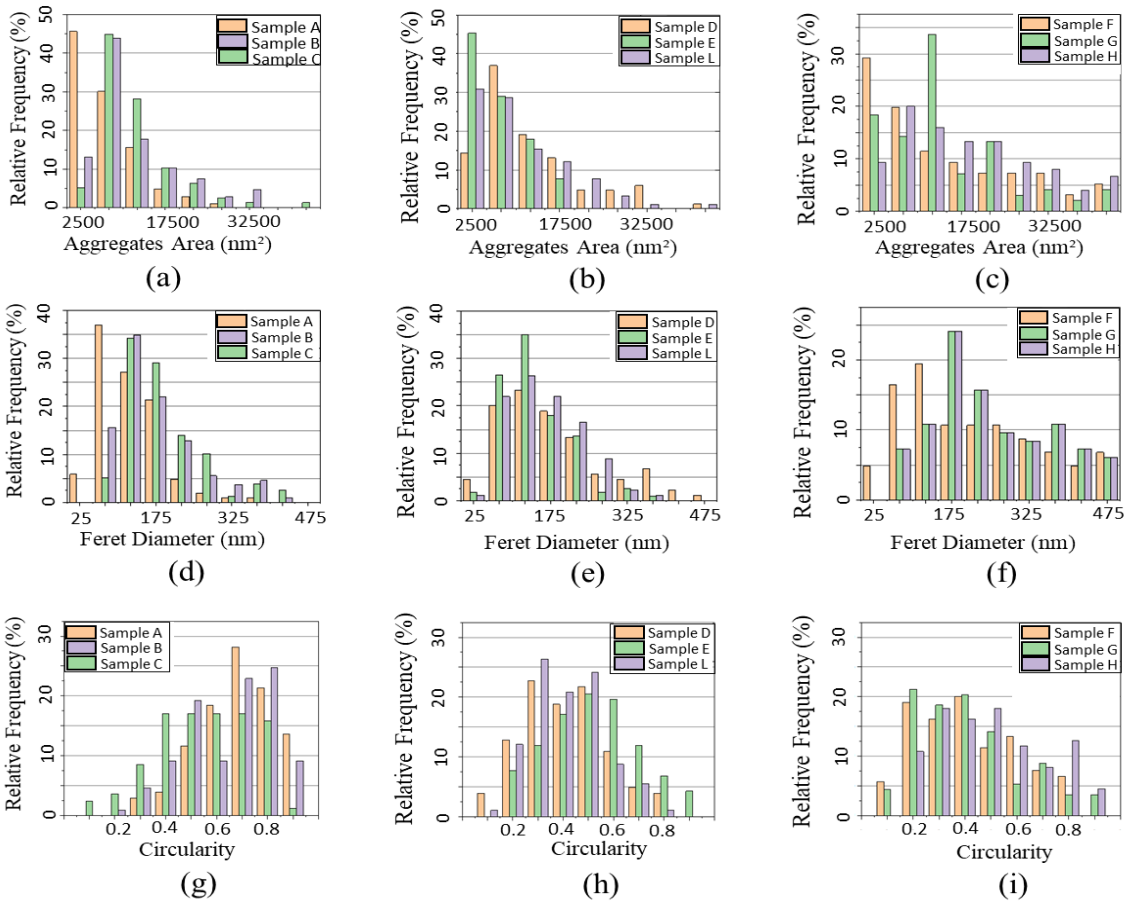

Figure 7: Distributions of the aggregates' area, Feret diameter and circularity of the tested samples.

3.2 XPS

An XPS analysis was carried out to further investigate the surface composition of the samples. While TEM and EDX were carried out on individual soot nanoparticles, XPS represents an average over the entire sample. The survey spectra for all those samples are shown in Figure 8, whereas the XPS survey data from the samples are listed in Table 3.

The XPS survey scans cover a wide energy range in which the chemical elements are identified based on the emitted photoelectron kinetic energy. Sample L is mostly composed of carbon, with a small amount of oxygen in its surface. The engine soot samples revealed greater chemical heterogeneity. The major component of soot in all engine samples is C, together with O and traces of N. Small amounts of the additive-derived elements Ca, S, Zn, and Mg were also detected on the soot surface, together with additional inorganic elements. As previously discussed, those metallic (Ca, Zn, Mg) and non-metallic (P, S, B) elements found in the particulate matter are likely to come from detergents, dispersants, antioxidants, and anti-wear agents typically used in the oil additive package [59, 83].

The C1s spectrum is particularly interesting since it reflects the degree of graphitization in the material. Figure 8b shows the C1s spectra of the samples under investigation. At the binding energy of 284.4 eV, there is a significant difference in their shape. Muller [60] showed that the full width at half maximum (FWHM) of the C1s signal decreases as the graphitization increases in the material. The spectra in Figure 8b are sorted according to the different graphitization found in the samples. From top (sample L) to bottom (Sample A) the FWHM increases suggesting a decrease in the structural order in the material.

1

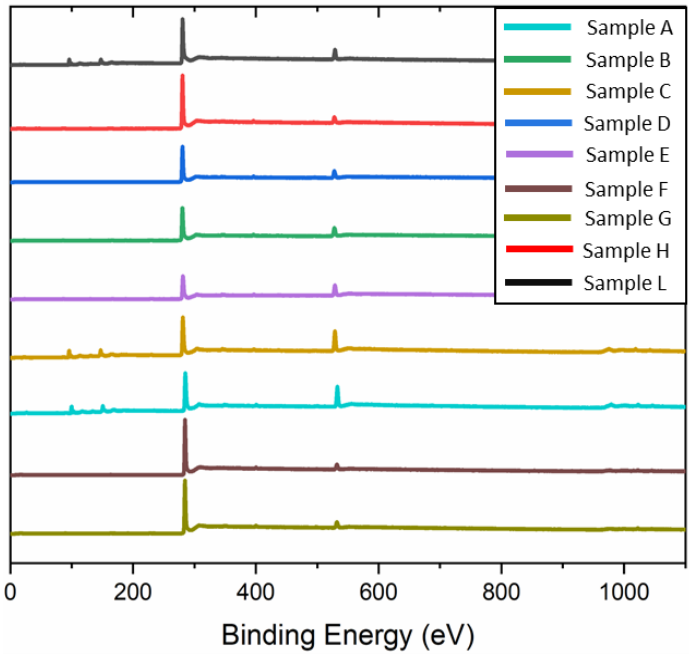

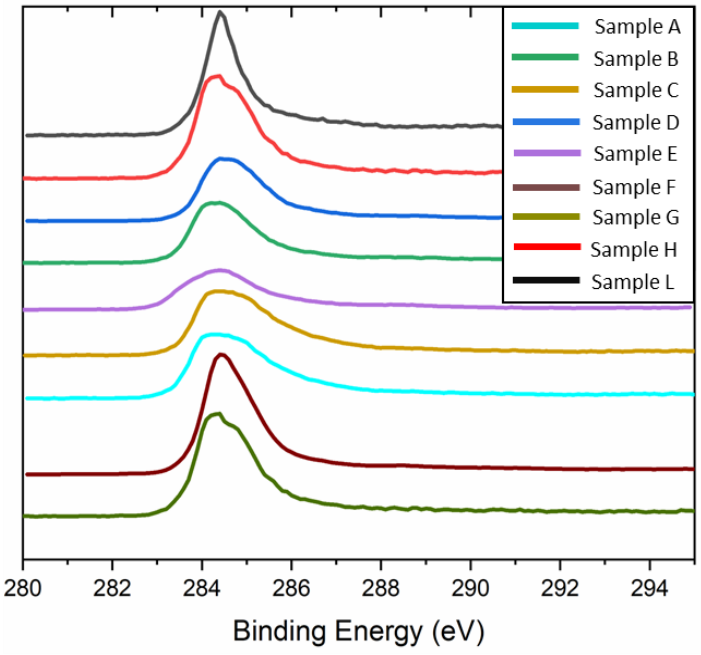

Sample	FWHM eV
Mogul L	0.87
Sample H	1.17
Sample F	1.29
Sample G	1.46
Sample D	1.60
Sample C	1.60
Sample B	1.64
Sample E	1.92
Sample A	2.03

Figure 8: XPS spectra of soot samples: (a) XPS survey spectra (b) XPS C1s core level spectra.

By deconvolution of a high-resolution scan over the nominal C1s energy region, carbon hybridization can be identified by the relative peak position and its concentration by the relative intensity of the corresponding peak [84, 85]. After a normalization at 284.4 eV, the carbon high-resolution spectra were processed by the Casa XPS software, using a four-band peak-fitting routine with Shirley background and symmetrical Gaussian – Lorentzian mixture of 70 and 30%, respectively. The carbon functional groups were calculated by integrating the appropriate peak intensities from high-resolution scans and normalising them to the integrated count intensity across the complete C1s spectrum for each soot sample. In three consecutive analyses, the intensities of peaks from any sample were found to be consistent, with differences of less than 5%.

Oxygen-to-carbon ratios and carbon hybridization (e.g. sp2/sp3 carbon) for all samples are reported in Table 4. The sp2/sp3 ratio, which is also used as indicator of structural order within a carbon material, decreases going from sample L to sample A, in agreement with L being less reactive than A. Thus, a general higher reactivity is suggested for samples which show a higher content of defects and oxygen on their surface.

Table 3: Surface chemical composition of the samples under investigation

Element	Sample A wt.%	Sample B wt.%	Sample C wt.%	Sample D wt.%	Sample E wt.%	Sample F wt.%	Sample G wt.%	Sample H wt.%	Sample L wt.%
C	77.44	84.09	89.71	91.53	81.68	96.09	93.32	93.57	97,5
O	12.98	11.96	9.27	7.29	13.29	3.68	4.42	5.32	2,5
Mg	1.24	1.54	0.93	0.86	1.4		0.74	0.59	
Zn	0.12	0.12	0.08	0.14	0.09	0.05		0.09	
Ca	0.55	0.68		0.18	0.63				
S	2.64				0.46	0.18	0.39	0.08	
N					1.5		0.98		
B	2.78	1.61			0.95		0.16	0.36	
P	1.32								
Al	0.69								
F	0.25								

Table 4: sp^2/sp^3 quantification and O/C ratio for the samples under investigation.

	Sample A	Sample B	Sample C	Sample D	Sample E	Sample F	Sample G	Sample H	Sample L
Carbon (%)	77.44	84.09	89.71	91.53	81.68	96.09	93.32	93.57	97.50
Oxygen (%)	12.98	11.96	9.27	7.29	13.29	3.68	4.42	5.32	2.50
Graphitic Carbon (%)	54.75	52.87	63.83	71.94	60.07	76.21	75.75	76.55	67.49
Aliphatic Carbon (%)	33.90	33.97	25.42	19.74	23.53	12.8	13.07	13.30	2.36
Sp2/Sp3 Ratio	1.62	1.55	2.51	3.64	2.55	5.95	5.80	5.75	28.60
O/C Ratio	0.17	0.14	0.10	0.08	0.16	0.04	0.05	0.06	0.03

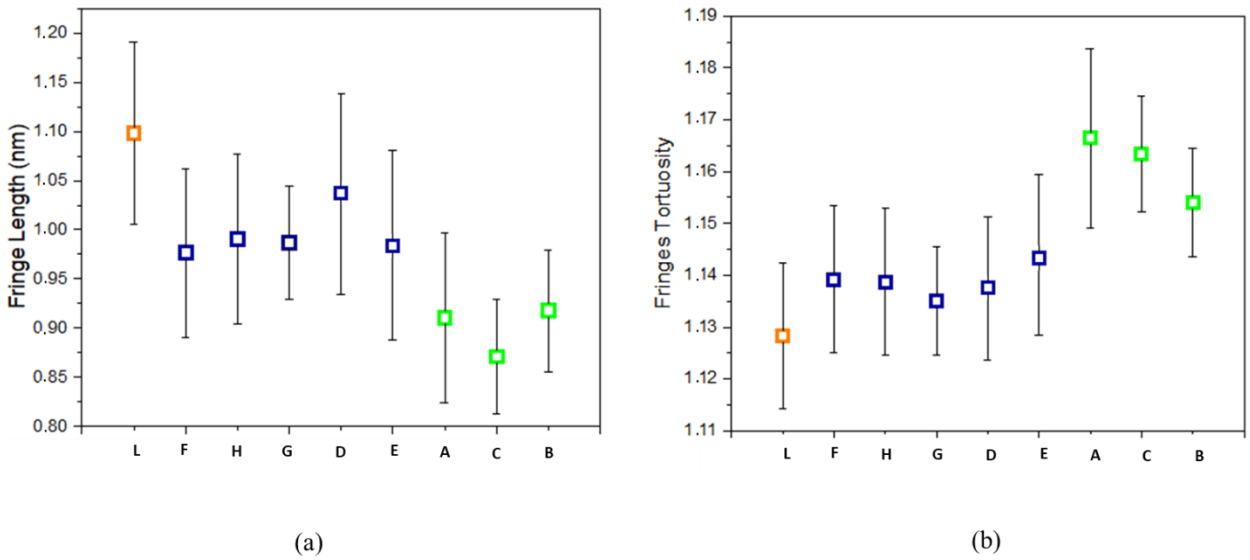

Figure 9: Comparison of the fringe length (a) and fringe tortuosity (b), obtained from fringe analysis of HRTEM images. The mean value is indicated by boxes with the markers indicating the standard deviation. Samples sorted from most graphitic to least graphitic. Sample L, (orange); more graphitic engine samples F, H, G, D and E (blue); and less graphitic engine samples A, C and B (green).

3.3 Fringes Analysis

Figure 9 illustrates the distributions of fringe lengths and tortuosity resulting from examination of HRTEM images. The computed values of these parameters for all the examined samples are likewise shown in Table 5. Sample L had the longest fringes of 1.10 nm. The average fringe length for the soot samples A, B and C was found to be significantly different, with 0.91 nm, 0.92 nm, and 0.87 nm, respectively. The gap between sample L and the remaining samples is approximately 0.11 nm, with an average fringe length of 0.99 nm (samples D-H). In comparison to the reference sample L, two classes of graphitization can thus be identified among the soot samples: medium and low-level graphitization. They appear to be related to the amount of soot in the oil and/or the source of the soot. Sample L is the most graphitic sample. The two engine soot classes, on the other hand, showed a 10% and 21% reduction in mean fringes length, respectively, when compared to sample L. These values agree with those reported in previous findings. Pfau et al. [62] found lamellae of about 1.08 nm in the soot extracted from the oil drain of two diesel engines. The carbon black sample showed instead longer fringes of about 1.13 nm. Similarly, in their investigation on thermal oxidation of different carbon blacks and diesel soot samples, Jaramillo [48] reported fringes lengths of about 0.98 nm in engine-derived soot. However, they also found shorter fringes lengths for the carbon black samples Monarch 1300 and Regal 250 (0.8-0.9 nm). In contrast, Seong found greater fringes extensions for carbon black in comparison to engine soot [86]. Longer engine soot fringes ranging from 1.16 to 1.2 nm have been found by Li [87] depending on the fuel injection strategy. Similarly, nanostructure

dependency upon injection timing was also observed by Xu and co-workers, with fringes lengths in the range 1.12-1.4 nm [45]. As pointed out by Pfau, soot-in-oil nanostructure is examined following the oil drainage and thereby it relies on the whole engine test conditions [62]. This would explain the variation in the fringes' properties across the engine samples in this investigation.

Sample L showed the least tortuous carbon fringes (mean value 1.13). The fringes of the most graphitic engine samples were found to have almost the same degree of tortuosity, with 1.14 for all samples (Table 5). More bent graphene layers have been found in the soot samples A-C, with a value of about 1.16. These findings are consistent with those reported by Pfau and colleagues for diesel soot-in-oil samples [62], however, they are slightly lower than those found in earlier investigations. Yehliu reported a mean fringe tortuosity in the range 1.12-1.37 depending on injection strategy and fuel formulation [29]. Less bent graphene layers have been measured by Xu and co-workers [45]. They found increased tortuosity values from 1.11 to 1.22 for lower fuel injection pressures. Similarly, Jaramillo [48] reported fringe tortuosities in the range 1.17-1.2. Rohani [88] measured fringe tortuosity up to 1.38 for soot samples collected from the exhaust of a single-cylinder diesel engine. Overall, a tortuosity range of 1.11-1.38 have been observed in the aforementioned works. The tortuosity range reported in this investigation lie in the lower part of this range. As pointed out by Pfau and Rohani [62, 88], the lower fringes tortuosities can be attributed to the lower degree of soot oxidation in the lubricating oil in comparison to the exhaust. Moreover, variables such as the TEM picture's quality and the algorithm used to detect the fringes might potentially contribute to the discrepancies found in literature. Overall, the samples examined in this investigation exhibit different nanostructure. Fringe analysis showed that sample L is the most graphitic sample, while samples A, B and C have the least ordered nanostructure. It Is generally accepted that the structural order has an impact on the soot oxidation reactivity [60, 89, 90]. Muller found increasing fringes tortuosities and shorter lengths for more oxidised samples [60]. A more disordered nanostructure increases the number of defect and thus resulting more prone to oxygen attack [66]. This assumption is supported by the present results.

Table 5: Mean length and tortuosity values of the graphene layers

Sample	Length nm	Tortuosity
Sample L	1.10 ± 0.09	1.13 ± 0.01
Sample F	0.98 ± 0.09	1.14 ± 0.01
Sample H	0.99 ± 0.09	1.14 ± 0.01
Sample G	0.99 ± 0.06	1.14 ± 0.01
Sample D	1.04 ± 0.10	1.14 ± 0.01
Sample E	0.98 ± 0.10	1.14 ± 0.02
Sample B	0.92 ± 0.09	1.15 ± 0.02
Sample C	0.87 ± 0.06	1.16 ± 0.01
Sample A	0.91 ± 0.06	1.17 ± 0.01

4. Discussion

In this study, we analysed soot-in-oil samples from a comprehensive set of sources namely, field-derived soot, dyno-derived soot, and carbon black to understand whether within each family differences or similarities can be found. Understanding these distinctions can assist explaining some of the discrepancies with soot induced wear typically found in the literature and ultimately support future engine oil additive packages and engine design in mitigating the influence of soot on wear. Although several factors such as fuel formulation [21, 91, 92], engine conditions [75, 78, 93], injection methods [45, 87], temperature [21, 92], EGR rates [26, 94, 95], and oil additive package [96] can influence soot characteristics, this investigation revealed some significant similarities and differences across diesel particulates. Different types of soot have been discovered based on their appearance under TEM and the extent of graphitization in the material. As a result, soot samples can be divided in two groups: class I (samples D-H) and class II (samples A-C). Sample L and the samples in class I, are similar in their appearance under TEM. Aggregates from class I samples are composed of distinct particles with a graphitic nanostructure and a typical diameter of about 18 nm. Sample L shows slightly bigger particulates with diameter of 22 nm. Class II particulates, on the other hand, exhibit a sludge like appearance. Their aggregates are formed by significantly smaller sludge-like aggregates, in which primary particles of 21 nm can be identified. In most samples, HRTEM was employed to analyse the primary particle nanostructure. While class I samples only differ slightly

from the highly graphitic carbon black, samples in class II show less ordered particulates' structures. Particulates with embedded metallic particles and more compact morphology were found in those samples as opposed to the modest chain-like geometry of the class I samples. Entirely amorphous particles were also observed in the samples A, B and C, with some showing crystalline formations. The source of these embedded structures, according to the EDX spectroscopy, was likely due to the lubricating oil additives and wear contaminants. Previous studies [56, 62, 97], have also observed "sludge-like" formations with embedded metallic material in soot samples drained from engine oil. Further investigation on the reasons/factors that promote this sludge-like soot formation in the field operation is needed.

The proportion of non-carbon content present in the soot samples is the second main difference between the engine-derived particulates. The graphitic structure of sample F (class I sample) has the lowest amount of oxygen-containing functional groups (3.68 %), whereas the highly defective samples E and C include the highest oxygen functionalities (~ 13%). Ca, S, Zn, P, and Mg are mainly attributable to additive package chemistry. The disorder in the carbon material is also shown by the FWHM of the C1s spectrum. This value decreases from 2.03 eV in the sample A to 1.17 eV for the sample H, indicating an increasing trend in carbon graphitization going from class II to class I samples. In an earlier investigation, Muller employed the same parameter to determine the degree of graphitization in carbon samples, establishing a strong connection between FWFM values and structural organization in the carbon material [60].

Information on the sp^2 and sp^3 carbon bonding percentages, along with oxygen functional groups, were determined by deconvolution of the XPS C1s spectra. The peak corresponds to sp^2 carbon (graphitic carbon) at approximately 284.4 eV, whereas the location at a binding energy of 285 eV is believed to be caused by defects in the carbon material [66]. Samples in class I, showed the highest degree of graphitization and correspondingly, the lowest oxygen content on soot surface. This is consistent with the observed higher number of defects and oxygen-to-carbon ratios have been found for the other samples (class II). The oxygen content has often been considered a critical factor in governing the soot oxidation mechanism [60, 98, 99]. Morjan [98] demonstrated how chemisorbed oxygen may be readily bound to the defective carbon edge sites, increasing the reactivity of the whole soot particle. In soot material, Muller [60] discovered a positive correlation between oxygen concentration and sp^3 carbon. The authors also proposed that oxygen functional species such as C = O and C-OH enhance total soot oxidation reactivity. Wang [99] also identified a connection between the soot activation energy and the concentration of aliphatic functional groups condensed on the soot surface.

Apart from the surface oxygen functional groups, the amount of the ash components, especially the metal species, appear to affect soot reactivity [100-103]. Jung [100] proposed that increased oil metal concentrations might promote soot oxidation, resulting in quicker and earlier oxidation. In their investigation on the effect of engine parameters and biodiesel content on the soot properties emitted by a four-cylinder diesel engine, Ess [101] have found a positive correlation between ash components (i.e., Fe, Cu and Zn) and oxidative reactivity of soot particles. The catalytic activity of those species in the soot oxidation process was used to explain the observed results. They also link the soot nanostructure with ash components, suggesting the latter as one of the main causes of soot structural disorder. This might be the case reported in this work, where the more disordered samples have greater ash component concentration.

The fringe analysis corroborated the greater disorder in the nanostructure of the class II samples. Among the samples, particulates in class I, have the longest fringes and, accordingly, the lowest tortuosity. Samples in class II, on the other hand, had the most structural disorder, with a 21% reduction in the mean fringe length when compared to the sample L. Long fringe lengths and modest fringe tortuosities are frequent characteristics of graphitic materials [21]. Thus, the samples in class I are more graphitic than those in class II.

A linear trend between carbon graphitization and oxygen content is evidenced in Figure 10. A higher oxygen content is associated to a lower graphitic order (shown as either fringes length or tortuosity) in the material. The higher oxygen level in sample E compared to the class I samples is likely to be associated with a higher ash content in the material (see tables 3 and 4), potentially leading to a higher carbon reactivity than expected for this material class [101].

Samples A, B and C have a more amorphous structure than the other engine samples, which provides them more edge sites and makes it more polar and reactive. This would suggest a greater degree of interaction between class II samples and the lubricating oil. As a result, the efficacy of oil additives may be increased, and wear may be reduced [15]. Moreover, greater soot reactivity to dispersant may result in improved soot dispersion in the oil and, therefore, improved wear protection in the event of oil starvation or abrasion wear process.

Moreover, the amorphous nature of particulates may play a key role in the wear process. Jenei et al. [104] observed a significant enhancement in soot hardness for particles exhibiting greater disorder. Similarly, Bhowmick reported that amorphous structures can increase particle hardness when subjected to compressive stress [105]. As a result, class II samples might behave more aggressively

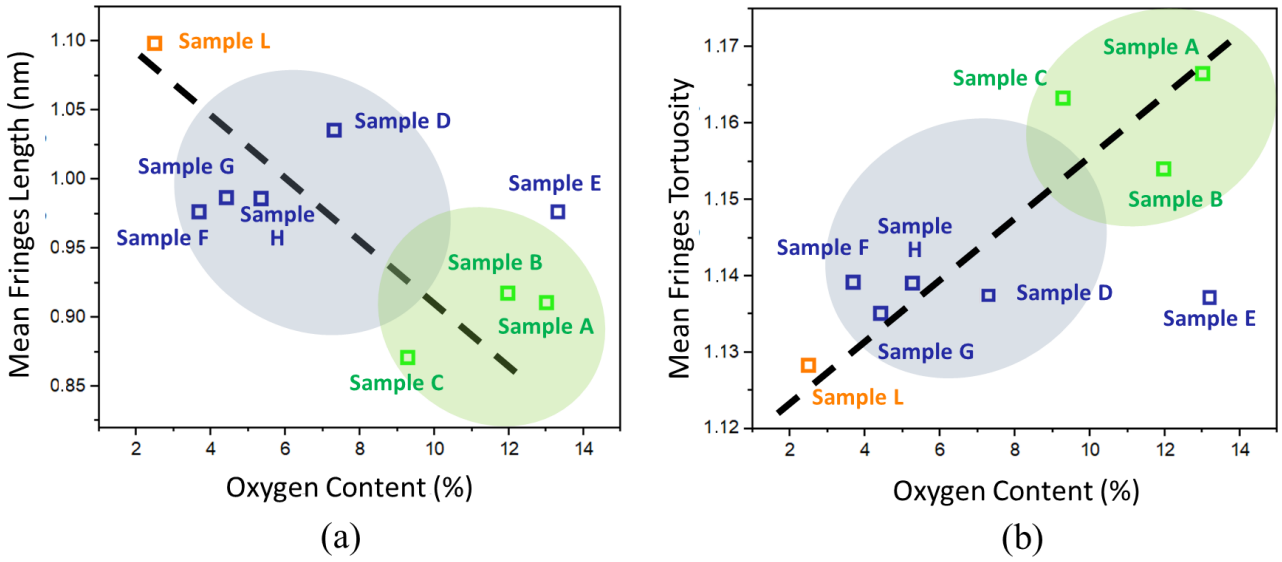

Figure 10: Correlation between surface oxygen content and fringes parameters. (a) mean fringes length; (b) mean fringes tortuosity. Raw XPS/fringe analysis data reported in the appendix.

when it comes to abrasive wear than class I samples. This emphasises how important it is to take into account the amorphous properties when understanding and predicting wear processes.

Oil viscosity has also been reported to be influenced by soot characteristics. Zeidan observed an increase in oil viscosity with higher soot loading and more compact particle shapes [106]. Bardasz et al. [41] reported reduced viscosity increase associated with higher dispersants levels in the oil. According to Esangbedo [15], rapid loss in oil viscosity control occurs in presence of graphitic/poor reactive soot particles in the oil.

Finally, many similarities have been found between sample L and samples in class I. Sample L exhibits the typical soot appearance under TEM microscope, with graphitic primary particles connected in branched or chain-like structures. Similar primary particle size and aggregate dimensions have also been measured for those samples; however, the chemical composition is the main difference.

Sample L is mostly composed of carbon, with a small amount of oxygen in its surface. Greater chemical heterogeneity was found in the engine soot samples attributed to the oil additive package contribution. Noticeably, low oxygen content and defective carbon have been found on carbon black surface, which may affect the reactivity and potentially the wear behaviour of this sample. These findings are consistent with those reported in previous research [56]. The similarities between carbon black and engine soot, according to Clague [42], can be attributed to the many similarities in their formation processes. However, as demonstrated by Yehliu [29] for various heat treatments, the nanostructure can significantly change dramatically depending upon the carbon black and sample

preparation. Because of the morphological and nanostructure similarities with most of the engine-derived soot, sample L can be used as an engine soot mimic for future research in these fields. However, because of the discrepancies in chemical composition observed between sample L and the samples in class II, more research is needed to ascertain whether they cause similar wear and follow similar wear mechanisms in ICEs engines. The differences highlighted in this work for the different types of soot may lead to different soot-induced wear levels/mechanism and therefore impact on the life of engine components. The primary source of the sludge-like forms observed in this study for class II samples are thought to be the byproducts of oil oxidation; further research is currently underway to corroborate this hypothesis.

5. Conclusions

In this work, the chemical and physical characteristics of different soot-containing engine oil drains have been widely investigated. The aim was to compare particulates coming from different sources, highlighting the main similarities and differences among the samples. A flame-generated carbon black sample was also included as a comparative soot surrogate in this study. The main conclusions can be summarized as follows:

- The morphology of class I samples and carbon black is comparable, with aggregates formed of distinct particles with a graphitic nanostructure of 18 nm in diameter. Smaller globular sludge-like aggregates were observed in samples A, B, and C. The dark regions discovered in those aggregates were ascribed to oil additives and wear compounds.

- The morphological analysis on soot aggregates revealed similar sizes for most of the samples. The mean Feret diameter fluctuated from 120 nm to 331 nm. Circularity was in the range of 0.41 to 0.64. Samples F, G and H show the biggest dispersions, probably affected by the small agglomerates within the samples. The major differences were observed for the particle circularity. Class II particulates showed globular structures and the greatest circularity.

- Fringes analysis was employed for quantifying the differences between particles with similar graphitic nanostructure. The fringe length varied among the soot classes, with class II soot showing the shortest lamellae of 0.87-0.92 nm and longer fringes for class I soot with 0.98-1.04 nm (+13.5%) as well as carbon black with 1.10 nm (+23.6%). Fringe curvature showed an increasing trend

between samples: carbon black showed the flattest fringes (1.13), class I soot in the mid-range (1.14), and class II soot the more bent lamellae (1.15-1.17).

- XPS inspections revealed higher non-carbon content on soot surface together with higher defective sp^3 carbon and aliphatic functional groups in class II samples compared to class I particulates. The high-resolution C1s peak provided a measure of the relative fractions of sp^2/sp^3 carbon. The sp^2 / defect ratio decreases going from sample L to class II samples. This result is consistent with the increase in O / C ratio and the corresponding reduction in the degree of graphitization in the material. This suggests a general higher reactivity for sample A which shows a higher content of defects and oxygen on its surface. A linear trend was found between surface oxygen content and the fringe length as well as the fringe tortuosity. This finding is consistent with the assumption that a more disordered nanostructure increases the number of defects, making it more susceptible to oxygen attack.

This work is part of an ongoing investigation which aims to contribute to understanding the differences between different soot types and their potential impact on oil performances and wear. The preliminary results suggest that different soot classes can exist based on the particulate appearance under TEM, soot nanostructure and chemical composition. Those differences seem to be related to soot origin (dyno vs field). This work suggests that carbon black may not always be an ideal mimic for tribological testing, as a consequence, it is advisable to fully characterise the carbon material before adopting it as a soot surrogate in tribological investigations. As a result, to determine the soot impact on engine performance and components, a rigorous analysis of the particulate characteristics is required.

Acknowledgements

The authors would like to thank Infineum UK Ltd and Volvo Group Trucks Technology for providing the oil samples and, for their support with engine setup and testing. The authors also thank the Nanoscale and Microscale Research Centre (nmRC) for providing access to instrumentation.

References

1. Kalghatgi, G., *Is it really the end of internal combustion engines and petroleum in transport?* Applied energy, 2018. **225**: p. 965-974.
2. Ekberg, K., L. Eriksson, and C. Sundström, *Electrification of a heavy-duty CI truck—Comparison of electric turbocharger and crank shaft motor.* Energies, 2021. **14**(5): p. 1402.
3. Yongzhi, C., Y. Xuekuan, and H. Yuhai. *Review of the Present Situation and Development of Marine Diesel Engine*. in *2017 International Conference on Industrial Informatics-Computing Technology, Intelligent Technology, Industrial Information Integration (ICIICII)*. 2017. IEEE.
4. Knecht, W., *Diesel engine development in view of reduced emission standards.* Energy, 2008. **33**(2): p. 264-271.
5. Fiebig, M., et al., *Particulate emissions from diesel engines: correlation between engine technology and emissions.* Journal of occupational medicine and toxicology, 2014. **9**(1): p. 1-18.
6. Tanin, K., et al., *The influence of boost pressure on emissions and fuel consumption of a heavy-duty single-cylinder DI diesel engine.* SAE transactions, 1999: p. 1198-1219.
7. Zhao, H., *Advanced direct injection combustion engine technologies and development: diesel engines*. Vol. 2. 2009: Elsevier.
8. Gomaa, M., A. Alimin, and K. Kamarudin, *Trade-off between NOx, Soot and EGR rates for an IDI diesel engine fuelled with JB5.* International Journal of Mechanical and Mechatronics Engineering, 2010. **4**(2): p. 196-201.
9. Dennis, A., C.P. Garner, and D. Taylor, *The effect of EGR on diesel engine wear.* SAE transactions, 1999: p. 1185-1197.
10. Aldajah, S., et al., *Effect of exhaust gas recirculation (EGR) contamination of diesel engine oil on wear.* Wear, 2007. **263**(1-6): p. 93-98.
11. Green, D. and R. Lewis, *The effects of soot-contaminated engine oil on wear and friction: a review.* Proceedings of the Institution of Mechanical Engineers, Part D: Journal of Automobile Engineering, 2008. **222**(9): p. 1669-1689.
12. Hu, E., et al., *The role of soot particles in the tribological behavior of engine lubricating oils.* Wear, 2013. **304**(1-2): p. 152-161.
13. Pacino, A., et al., *Understanding the Challenges Associated with Soot-in-Oil from Diesel Engines: A Review Paper.* 2021.
14. Kirkby, T., et al., *Soot wear mechanisms in heavy-duty diesel engine contacts.* Wear, 2023. **524**: p. 204733.
15. Esangbedo, C., A.L. Boehman, and J.M. Perez, *Characteristics of diesel engine soot that lead to excessive oil thickening.* Tribology International, 2012. **47**: p. 194-203.
16. Omidvarborna, H., A. Kumar, and D.-S. Kim, *Recent studies on soot modeling for diesel combustion.* Renewable and Sustainable Energy Reviews, 2015. **48**: p. 635-647.
17. Kittelson, D.B., J.L. Ambs, and H. Hadjkacem, *Particulate emissions from diesel engines: influence of in-cylinder surface.* SAE transactions, 1990: p. 1457-1472.

18. Suhre, B.R. and D.E. Foster, *In-cylinder soot deposition rates due to thermophoresis in a direct injection diesel engine.* SAE transactions, 1992: p. 1648-1661.
19. Mahmood, W.M.F.W., et al., *Predicted paths of soot particles in the cylinders of a direct injection diesel engine*. 2012, SAE Technical Paper.
20. Vander Wal, R.L., et al., *Analysis of HRTEM images for carbon nanostructure quantification.* Journal of Nanoparticle Research, 2004. **6**(6): p. 555-568.
21. Vander Wal, R.L. and A.J. Tomasek, *Soot oxidation: dependence upon initial nanostructure.* Combustion and flame, 2003. **134**(1-2): p. 1-9.
22. Gogoi, B., et al., *Effects of 2, 5-dimethylfuran addition to diesel on soot nanostructures and reactivity.* Fuel, 2015. **159**: p. 766-775.
23. Ma, Z., et al., *Effects of diesel oxidation catalyst on nanostructure and reactivity of diesel soot.* Energy & Fuels, 2014. **28**(7): p. 4376-4382.
24. Marsh, H. and K. Kuo, *Kinetics and catalysis of carbon gasification*, in *Introduction to carbon science*. 1989, Elsevier. p. 107-151.
25. Pfau, S.A., A. La Rocca, and M.W. Fay, *Quantifying soot nanostructures: Importance of image processing parameters for lattice fringe analysis.* Combustion and Flame, 2020. **211**: p. 430-444.
26. Al-Qurashi, K. and A.L. Boehman, *Impact of exhaust gas recirculation (EGR) on the oxidative reactivity of diesel engine soot.* Combustion and Flame, 2008. **155**(4): p. 675-695.
27. Bogarra, M., et al., *Influence of on-board produced hydrogen and three way catalyst on soot nanostructure in Gasoline Direct Injection engines.* Carbon, 2017. **120**: p. 326-336.
28. Sharma, V., et al., *Structure and chemistry of crankcase and exhaust soot extracted from diesel engines.* Carbon, 2016. **103**: p. 327-338.
29. Yehliu, K., R.L. Vander Wal, and A.L. Boehman, *A comparison of soot nanostructure obtained using two high resolution transmission electron microscopy image analysis algorithms.* Carbon, 2011. **49**(13): p. 4256-4268.
30. Vander Wal, R.L., V.M. Bryg, and M.D. Hays, *Fingerprinting soot (towards source identification): Physical structure and chemical composition.* Journal of Aerosol Science, 2010. **41**(1): p. 108-117.
31. Corso, S. and R. Adamo, *The effect of diesel soot on reactivity of oil additives and valve train materials*. 1984, SAE Technical Paper.
32. Gautam, M., et al., *Contribution of soot contaminated oils to wear.* SAE transactions, 1998: p. 598-621.
33. Hosonuma, K., K. Yoshida, and A. Matsunaga, *The decomposition products of zinc dialkyldithiophosphate in an engine and their interaction with diesel soot.* Wear, 1985. **103**(4): p. 297-309.
34. Kawamura, M., et al., *Deterioration of antiwear properties of diesel engine oils during use.* Wear, 1988. **123**(3): p. 269-280.
35. Rounds, F.G., *Soots from used diesel-engine oils: their effects on wear as measured in 4-ball wear tests*. 1981, Society of Automotive Engineers, Inc., Warrendale, PA.
36. Sato, H., et al., *Study on wear mechanism by soot contaminated in engine oil (first report: relation between characteristics of used oil and wear)*. 1999, SAE Technical Paper.
37. Green, D. and R. Lewis, *Effect of soot on oil properties and wear of engine components.* Journal of physics D: Applied physics, 2007. **40**(18): p. 5488.
38. Antusch, S., et al., *On the tribochemical action of engine soot.* Wear, 2010. **269**(1-2): p. 1-12.
39. George, S., S. Balla, and M. Gautam, *Effect of diesel soot contaminated oil on engine wear.* Wear, 2007. **262**(9-10): p. 1113-1122.
40. Motamen Salehi, F., et al., *Corrosive–abrasive wear induced by soot in boundary lubrication regime.* Tribology Letters, 2016. **63**(2): p. 1-11.
41. Bardasz, E.A., et al., *Understanding Soot Mediated Oil Thickening Through Designed Experimentation Part 2: GM 6.5 L.* SAE transactions, 1996: p. 1320-1331.

42. Clague, A., et al., *A comparison of diesel engine soot with carbon black.* Carbon, 1999. **37**(10): p. 1553-1565.
43. Booth, J., et al., *The feasibility of using electrostatic monitoring to identify diesel lubricant additives and soot contamination interactions by factorial analysis.* Tribology international, 2006. **39**(12): p. 1564-1575.
44. Green, D. and R. Lewis, *Investigation of soot contaminated lubricant wear mechanisms*. 2007, SAE Technical Paper.
45. Xu, Z., et al., *Effects of injection timing on exhaust particle size and nanostructure on a diesel engine at different loads.* Journal of aerosol science, 2014. **76**: p. 28-38.
46. Zhu, J., et al., *Effects of engine operating conditions on morphology, microstructure, and fractal geometry of light-duty diesel engine particulates.* Proceedings of the Combustion Institute, 2005. **30**(2): p. 2781-2789.
47. Wedlock, D.J., et al., *Experimental and simulation approaches to understanding soot aggregation*. 1999, SAE Technical Paper.
48. Jaramillo, I.C., et al., *Effect of nanostructure, oxidative pressure and extent of oxidation on model carbon reactivity.* Combustion and Flame, 2015. **162**(5): p. 1848-1856.
49. Li, S., et al., *Wear in Cummins M-11/EGR test engines.* SAE Transactions, 2002: p. 2258-2271.
50. Bhowmick, H. and S. Biswas, *Tribology of ethylene–air diffusion flame soot under dry and lubricated contact conditions.* Journal of Physics D: Applied Physics, 2011. **44**(48): p. 485401.
51. Jao, T.C., et al., *Soot characterisation and diesel engine wear.* Lubrication Science, 2004. **16**(2): p. 111-126.
52. Skurai, T. and K. Yoshida. *Tribological behaviour of dispersed phase systems*. in *International Tribology Conference*. 1987.
53. Olomolehin, Y., R. Kapadia, and H. Spikes, *Antagonistic interaction of antiwear additives and carbon black.* Tribology Letters, 2010. **37**: p. 49-58.
54. Berbezier, I., J. Martin, and P. Kapsa, *The role of carbon in lubricated mild wear.* Tribology International, 1986. **19**(3): p. 115-122.
55. Mainwaring, R., *Soot and wear in heavy duty diesel engines.* SAE transactions, 1997: p. 1721-1738.
56. Uy, D., et al., *Characterization of gasoline soot and comparison to diesel soot: morphology, chemistry, and wear.* Tribology International, 2014. **80**: p. 198-209.
57. La Rocca, A., et al., *The nanostructure of soot-in-oil particles and agglomerates from an automotive diesel engine.* Tribology International, 2013. **61**: p. 80-87.
58. Escribano, R., et al., *Raman spectroscopy of carbon-containing particles.* Vibrational Spectroscopy, 2001. **26**(2): p. 179-186.
59. Kim, K., et al., *Characterization of engine oil additive packages on diesel particulate emissions.* Journal of Mechanical Science and Technology, 2020. **34**(2): p. 931-939.
60. Müller, J.-O., et al., *Bulk and surface structural investigations of diesel engine soot and carbon black.* Physical Chemistry Chemical Physics, 2007. **9**(30): p. 4018-4025.
61. Patel, M. and P.B. Aswath, *Structure and chemistry of crankcase and cylinder soot and tribofilms on piston rings from a Mack T-12 dynamometer engine test.* Tribology International, 2014. **77**: p. 111-121.
62. Pfau, S.A., et al., *Comparative nanostructure analysis of gasoline turbocharged direct injection and diesel soot-in-oil with carbon black.* Carbon, 2018. **139**: p. 342-352.
63. Sadezky, A., et al., *Raman microspectroscopy of soot and related carbonaceous materials: Spectral analysis and structural information.* Carbon, 2005. **43**(8): p. 1731-1742.
64. Vyavhare, K., et al., *Impact of diesel engine oil additives–soot interactions on physiochemical, oxidation, and wear characteristics of soot.* Energy & Fuels, 2019. **33**(5): p. 4515-4530.

65. Haffner-Staton, E., et al., *Morphological characterization of gasoline soot-in-oil: Development of semi-automated 2D-TEM and comparison with novel high-throughput 3D-TEM*. 2019, SAE Technical Paper.
66. Vander Wal, R.L., V.M. Bryg, and M.D. Hays, *XPS analysis of combustion aerosols for chemical composition, surface chemistry, and carbon chemical state.* Analytical chemistry, 2011. **83**(6): p. 1924-1930.
67. Guo, S., et al., *Comparability of Raman spectroscopic configurations: a large scale cross-laboratory study.* Analytical Chemistry, 2020. **92**(24): p. 15745-15756.
68. Fay, M., A. La Rocca, and P. Shayler. *TEM and HRTEM of Soot-in-oil particles and agglomerates from internal combustion engines*. in *Journal of Physics: Conference Series*. 2014. IOP Publishing.
69. La Rocca, A., et al., *Application of nanoparticle tracking analysis platform for the measurement of soot-in-oil agglomerates from automotive engines.* Tribology International, 2014. **70**: p. 142-147.
70. La Rocca, A., et al., *Characterisation of soot in oil from a gasoline direct injection engine using Transmission Electron Microscopy.* Tribology International, 2015. **86**: p. 77-84.
71. Neer, A. and U.O. Koylu, *Effect of operating conditions on the size, morphology, and concentration of submicrometer particulates emitted from a diesel engine.* Combustion and flame, 2006. **146**(1-2): p. 142-154.
72. Uy, D., et al., *Soot–additive interactions in engine oils.* Lubrication Science, 2010. **22**(1): p. 19-36.
73. Pacino, A., et al., *Investigating the morphology and nanostructure of carbon black dispersed in lubricant oils and their impact on chain wear as a proxy of marginally lubricated components*. 2023, Society of Automotive Engineers of Japan.
74. Kondo, K., et al., *Uncertainty in sampling and TEM analysis of soot particles in Diesel spray flame*. 2013, SAE Technical Paper.
75. Lapuerta, M., F.J. Martos, and J.M. Herreros, *Effect of engine operating conditions on the size of primary particles composing diesel soot agglomerates.* Journal of aerosol science, 2007. **38**(4): p. 455-466.
76. Su, D.S., et al., *Microstructure and oxidation behaviour of Euro IV diesel engine soot: a comparative study with synthetic model soot substances.* Catalysis today, 2004. **90**(1-2): p. 127-132.
77. Lee, K.O., et al., *Morphological investigation of the microstructure, dimensions, and fractal geometry of diesel particulates.* Proceedings of the Combustion Institute, 2002. **29**(1): p. 647-653.
78. Lu, T., C.S. Cheung, and Z. Huang, *Effects of engine operating conditions on the size and nanostructure of diesel particles.* Journal of Aerosol Science, 2012. **47**: p. 27-38.
79. Medalia, A.I., *Morphology of aggregates: I. Calculation of shape and bulkiness factors; application to computer-simulated random flocs.* Journal of Colloid and Interface Science, 1967. **24**(3): p. 393-404.
80. Orhan, O., et al., *Characterisation of flame-generated soot and soot-in-oil using electron tomography volume reconstructions and comparison with traditional 2D-TEM measurements.* Tribology International, 2016. **104**: p. 272-284.
81. Bagi, S., et al., *Multiscale characterization of exhaust and crankcase soot extracted from heavy-duty diesel engine and implications for DPF ash.* Fuel, 2020. **282**: p. 118878.
82. Sielicki, P., et al., *Grain type and size of particulate matter from diesel vehicle exhausts analysed by transmission electron microscopy.* Environmental technology, 2012. **33**(15): p. 1781-1788.
83. Zhang, Z., et al., *Interaction of ZDDP with borated dispersant using XANES and XPS.* Tribology transactions, 2004. **47**(4): p. 527-536.

84. Kaciulis, S., *Spectroscopy of carbon: from diamond to nitride films.* Surface and Interface Analysis, 2012. **44**(8): p. 1155-1161.
85. Chen, X., X. Wang, and D. Fang, *A review on C1s XPS-spectra for some kinds of carbon materials.* Fullerenes, Nanotubes and Carbon Nanostructures, 2020. **28**(12): p. 1048-1058.
86. Seong, H.J. and A.L. Boehman, *Evaluation of Raman parameters using visible Raman microscopy for soot oxidative reactivity.* Energy & Fuels, 2013. **27**(3): p. 1613-1624.
87. Li, X., et al., *Effect of multiple-injection strategies on diesel engine exhaust particle size and nanostructure.* Journal of Aerosol Science, 2015. **89**: p. 69-76.
88. Rohani, B. and C. Bae, *Morphology and nano-structure of soot in diesel spray and in engine exhaust.* Fuel, 2017. **203**: p. 47-56.
89. Johansson, K., et al., *Evolution of maturity levels of the particle surface and bulk during soot growth and oxidation in a flame.* Aerosol Science and Technology, 2017. **51**(12): p. 1333-1344.
90. Müller, J.-O., et al., *Diesel engine exhaust emission: oxidative behavior and microstructure of black smoke soot particulate.* Environmental science & technology, 2006. **40**(4): p. 1231-1236.
91. Lapuerta, M., O. Armas, and J.M. Herreros, *Emissions from a diesel–bioethanol blend in an automotive diesel engine.* Fuel, 2008. **87**(1): p. 25-31.
92. Yehliu, K., et al., *Impact of fuel formulation on the nanostructure and reactivity of diesel soot.* Combustion and Flame, 2012. **159**(12): p. 3597-3606.
93. Lee, K.O., et al., *Detailed characterization of morphology and dimensions of diesel particulates via thermophoretic sampling*. 2001, SAE Technical Paper.
94. Al-Qurashi, K., A.D. Lueking, and A.L. Boehman, *The deconvolution of the thermal, dilution, and chemical effects of exhaust gas recirculation (EGR) on the reactivity of engine and flame soot.* Combustion and Flame, 2011. **158**(9): p. 1696-1704.
95. Li, X., et al., *Impact of exhaust gas recirculation (EGR) on soot reactivity from a diesel engine operating at high load.* Applied Thermal Engineering, 2014. **68**(1-2): p. 100-106.
96. Gligorijevic, R., J. Jevtic, and D. Borak, *Engine oil contribution to diesel exhaust emissions.* Journal of Synthetic Lubrication, 2006. **23**(1): p. 27-38.
97. Pfau, S.A., et al., *Soot in the lubricating oil: an overlooked concern for the gasoline direct injection engine?* SAE Technical Papers, 2019. **2019**.
98. Morjan, I., et al., *Gas composition in laser pyrolysis of hydrocarbon-based mixtures: Influence on soot morphology.* Carbon, 2004. **42**(7): p. 1269-1273.
99. Wang, L., et al., *Aliphatic C–H and oxygenated surface functional groups of diesel in-cylinder soot: Characterizations and impact on soot oxidation behavior.* Proceedings of the Combustion Institute, 2013. **34**(2): p. 3099-3106.
100. Jung, H., D.B. Kittelson, and M.R. Zachariah, *The influence of engine lubricating oil on diesel nanoparticle emissions and kinetics of oxidation*. 2003, SAE Technical Paper.
101. Ess, M.N., et al., *Reactivity and structure of soot generated at varying biofuel content and engine operating parameters.* Combustion and Flame, 2016. **163**: p. 157-169.
102. Hansen, B.B., A.D. Jensen, and P.A. Jensen, *Performance of diesel particulate filter catalysts in the presence of biodiesel ash species.* Fuel, 2013. **106**: p. 234-240.
103. Johnson, T.V., *Review of vehicular emissions trends.* SAE International Journal of Engines, 2015. **8**(3): p. 1152-1167.
104. Jenei, I.Z., et al., *Mechanical response of gasoline soot nanoparticles under compression: An in situ TEM study.* Tribology International, 2019. **131**: p. 446-453.
105. Bhowmick, H. and S. Biswas, *Relationship between physical structure and tribology of single soot particles generated by burning ethylene.* Tribology Letters, 2011. **44**: p. 139-149.
106. Zeidan, M., et al., *Simulation of aggregation with applications to soot laden lubricating fluids.* Particle & Particle Systems Characterization: Measurement and Description of Particle Properties and Behavior in Powders and Other Disperse Systems, 2004. **21**(6): p. 473-482.

516

517

518

519

520